1 Introduction

A worldwide effort to directly detect gravitational radiation with large scale laser interferometers has been underway for the past several decades. In the United States the Laser Interferometer Gravitational-Wave Observatories (LIGO) have been operating since the early 2000's. During this time of operation a significant amount of effort was invested by the LIGO Scientific Collaboration to research, design, and build upgrades to the initial LIGO interferometers. As of 2011 the initial LIGO detectors were decommissioned and installation of these upgrades began. As installation has progressed the integration and commissioning phase has begun for many of the upgraded subsystems at the LIGO observatories.

One of the subsystems undergoing a significant upgrade for the Advanced LIGO era is the input optics. It is the task of the input optics to clean and stabilize the laser beam from the Pre-Stabilized Laser (PSL) before injection into the main interferometer. The upgraded sensitivity of the Advanced LIGO interferometers places stringent requirements on the stability of the input light and therefore on the input optics. In particular, the input optics must supply multiple low amplitude and phase noise RF sidebands. They must provide a frequency reference stable enough to not spoil the interferometer's gravitational wave sensitivity. They must provide mode matching and beam pointing actuation into the interferometer. Finally, they must provide isolation between the interferometer's reflected light and the input optics chain.

The next section of this paper, section II, will present the design requirements for the input optics and briefly explain how these requirements were derived. It will also describe some of the other Advanced LIGO subsystems in only as much detail as is necessary for an understanding of the input optics. Sections III and IV will give an overview description of the out-of-vacuum and in-vacuum components respectively. Section V will discuss the input mode cleaner which is at the heart of the input optics, both in location and form. Section VI will describe the Faraday Isolator whose design is highly customized for high power operation. Finally, sections VII and IIX will close with a description of the overall power throughput of the input optics chain and some conclusions.

2 Design Requirements

The design requirements for the input optics subsystem derive from the designed sensitivity of the interferometer. Figure 1 shows the design sensitivity

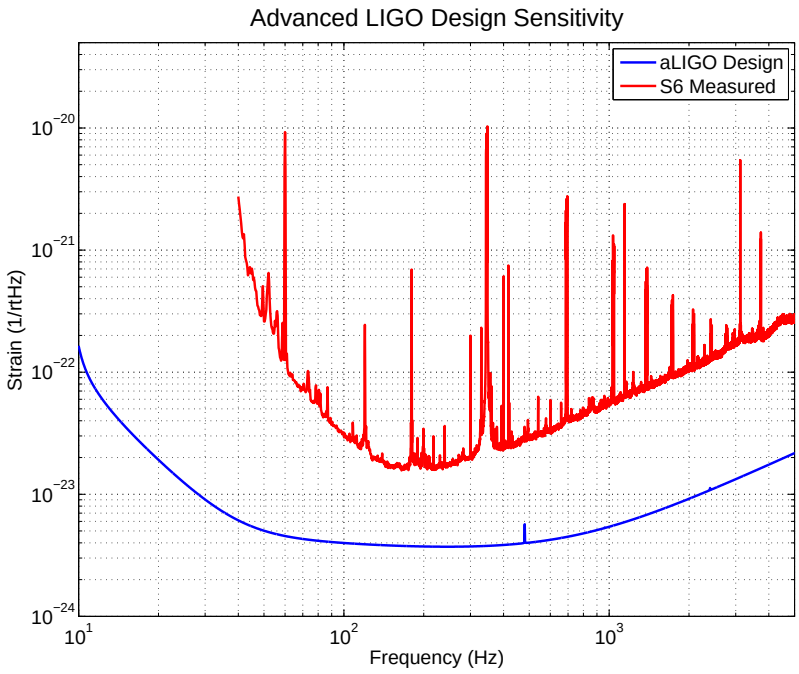

Figure 1: The Advanced LIGO design sensitivity[12] is shown together with the measured sensitivity from the LIGO Hanford Observatory during the sixth LIGO science run[11]. The design sensitivity includes the fundamental limiting noise sources (quantum, thermal, and seismic) which set the requirements for the interferometer subsystems such as the input optics.

of the Advanced LIGO interferometers together with the measured sensitivity of one of the Initial LIGO interferometers during the sixth science run. The Advanced LIGO interferometers are designed to be limited by seismic noise below ∼10 Hz, radiation pressure noise in the 10-50 Hz range, coating thermal noise between 50 Hz and 200 Hz, and photon shot noise above 200 Hz. The mantra for setting design requirements for the interferometer subsystems is therefore to keep the 'technical noise sources' below this limit. In fact the subsystem requirements were set by demanding that the technical noise sources be a factor of 10 below the design sensitivity[1].

2.1 Frequency Noise at the Interferometer Input

A perfect Michelson interferometer is completely insensitive to frequency noise; a fact which is a large motivator in choosing the Michelson topology for gravitational wave interferometers. However any asymmetry between the two arms of the Michelson interferometer will couple frequency fluctuations to the

output. The asymmetries between the two arms depend on many parameters such as: the imbalance between the reflectivity and transmissivity of the beam splitter, the reflectivity imbalance of the arm cavity input mirrors, different amounts of losses in the two arm cavities, and the static distance asymmetry between the beam splitter and the two arm cavities (known as the Schnupp asymmetry).

Using experience from Initial LIGO and a reasonable estimate of the Advanced LIGO parameters, the Interferometer Sensing and Control (ISC) group put together a detailed numerical simulation of the full Advanced LIGO interferometer [1]. With this simulation they derive the frequency noise requirement at the input to the interferometer to be roughly the curve labeled 'Frequency Noise Requirements at Interferometer Input' in figure 2. The frequency noise stabilization for the interferometer is not solely the job of the input optics; the final stabilization reference is the average length of the two arms. Figure 2 also shows the frequency noise requirements after suppression by the common arm length feedback servo. Also shown are the expected length noise of the input mode cleaner as well as the expected frequency noise out of the pre-stabilized laser.

The job of the input optics is therefore to stabilize the laser frequency by roughly a factor of 20 between 10 Hz and 10 kHz. In reality the frequency noise suppression necessary for the input optics is higher because acoustic effects in the injection chain will add frequency noise before the light is injected to the isolated in-vacuum optics.

2.2 Beam Alignment Noise at the Interferometer Input

As with frequency noise, a perfect Michelson interferometer is first order insensitive to pointing noise. There are two types of imperfections which couple pointing noise to the gravitational wave readout channel. The first considered in [10] is caused by residual misalignments of the core interferometer optics causing the misaligned beam to rejoin with the main interferometer mode and show up in the gravitational wave channel. The second coupling is caused by the beam spot motion on the core interferometer optics causing the residual angular motion of the optics to couple to the gravitational wave channel. These two effects lead to similar noise requirements at the input to the interferometer which a beam stability of $4 \cdot 10^{-10}$ $\frac{rad}{\sqrt{Hz}}$ at 100 Hz and above and decreasing (getting less stringent) as f^2 below 100 Hz.

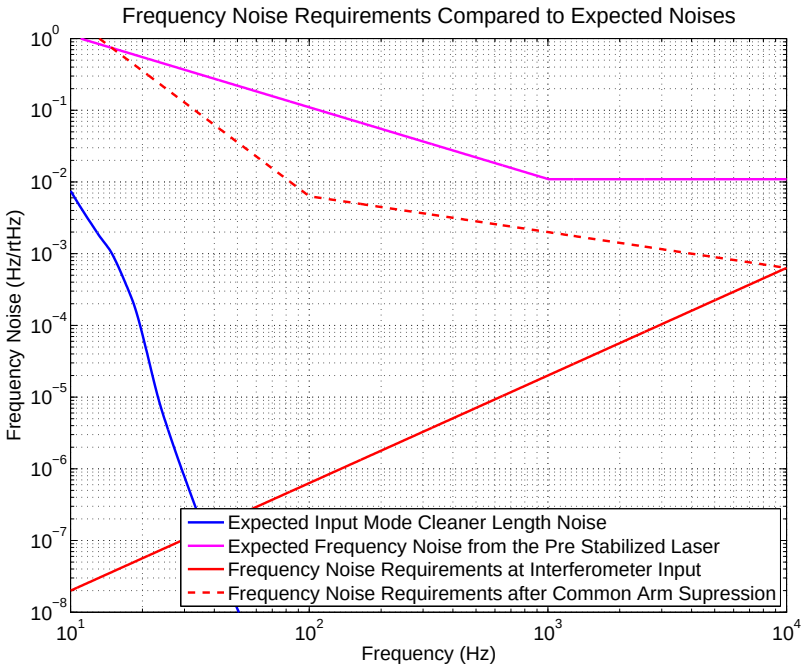

Figure 2: The rough frequency noise requirements at the input to the interferometer are shown both with and without the common arm loop suppression. Also shown are the expected length noise of the input mode cleaner and the expected frequency noise out of the pre-stabilized laser (PSL). Ostensibly the job of the input optics is to suppress the frequency noise out of the PSL to the requirements level after the common arm gain is taken into account. In reality acoustic effects in the injection optics between the PSL and the in-vacuum input optics will require a higher level of suppression.

2.3 RF Sidebands

Sensing and controlling most of the seven degrees of freedom of the interferometer are done by some variant of the Pound Drever Hall technique [5]. This technique uses optical heterodyne detection to sense the phase of the returning light from an optical cavity by sensing the phase modulation to amplitude modulation conversion which occurs when the cavity is slightly off resonance. It depends on having low noise radio frequency sidebands to generate detectable beat notes with the carrier light. It is part of the responsibility of the input optics to add these RF sidebands to the laser beam before delivering it to the interferometer.

In particular the input optics are responsible for adding three RF sidebands, one for controlling length of the input mode cleaner and two for controlling the other degrees of freedom of the interferometer. The phase modulator must be able to produce phase modulation depths up to 0.8, and must maintain a residual amplitude modulation level below $1 \cdot 10^{-4}$ $\frac{AM}{PM}$ ratio.

2.4 In-Vacuum Optical Isolation

The input optics is also required to provide isolation from the light reflected off of the interferometer. This is necessary to avoid inadvertently forming an optical cavity between the components of the input optics and the rest of the interferometer, an effect usually referred to as parasitic interferometry. Based on experience with parasitic interferometers in initial LIGO and power scaling arguments the isolation requirement level was set at 30 dB[3].

2.5 Throughput and Availability

The final requirements on the input optics are placed on the amount of light which is delivered to the interferometer and the amount of time which the input mode cleaner is available. In order to deliver the 125 W of laser power required for full power operation the input optics must achieve 75% throughput at all power levels including static and thermal mode matching losses. Additionally, in order not to spoil the detection availability of the interferometer it is required that the input mode cleaner re-lock time be less than 20 seconds.

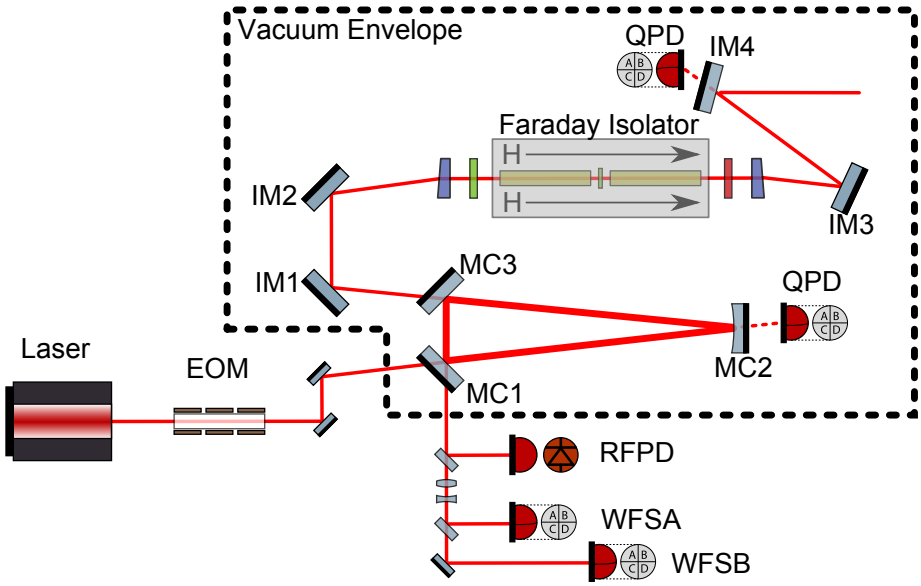

Figure 3: A schematic layout of the input optics[6]. The input mode cleaner is represented by the three mirrors MC1, MC2, and MC3. It is an in vacuum, triply suspended, triangular cavity used as a frequency and pointing reference. It also passively filters the spatial structure and polarization of the transmitted beam.

3 Input Mode Cleaner

The input mode cleaner is the heart of the input optics, serving simultaneously as a spatial filter, polarization filter, frequency reference, and pointing reference. It is an in-vacuum, suspended, three mirror cavity with the mirrors hanging from the LIGO small triple suspensions **citation**. It has a free spectral range of 9.099 MHz and a finesse of 515. The beam is injected along one of the long arms and extracted along the other (see 3). The reflected beam is outfitted with an RF photodiode for Pound-Drever-Hall length sensing **citation** and two differential wavefront sensors for angular control. In addition, a pickoff of the intra-cavity light is extracted behind the curved mirror, MC2, and sent to a quadrant photodiode for additional angular information.

3.1 Length Control

Defining the reflectivity of MC1 and MC3 to be r and assuming the cavity is lossless such that $t^2 = 1 - r^2$ we can express the complex reflectivity of the

cavity as

$$r_{IMC} = \frac{r(1 + e^{-i\phi})}{1 + r^2 e^{-i\phi}}, \tag{1}$$

where ϕ is the round trip phase given by

$$\phi = \tfrac{L}{c}\omega + (n + m)\psi + mod_2(n)\pi. \tag{2}$$

Here L represents the round trip length, c the speed of light, ω the laser frequency, ψ the round trip Gouy phase of the fundamental mode, and m/n the mode index of the TEM mode in question. Notice that this expression is identical to that of a 2 mirror impedance matched cavity except for the opposite sign in the denominator due to an odd number of mirrors.

The most important aspect of this expression for our purposes is that the reflection coefficient undergoes a very rapid phase change from $-\pi/2$ on one side of the resonance to $\pi/2$ on the other side of the resonance, analogously to mechanical oscillators. This phase change can be detected by measuring the beat note between the light passing through resonance and a pair of RF sidebands. This technique is known as the Pound-Drever-Hall technique[4][5] and allows for a very precise comparison between the length of the cavity and the frequency of the carrier light.

As discussed in the requirements section 2 one of the primary goals of the input optics is to quiet the laser frequency by at least an order of magnitude between 10 Hz and 10 kHz2. It is important however that the input optics not impress the length noise of the input mode cleaner at low frequencies where the laser frequency is much quieter. For this reason the cavity feedback servo is designed to servo the length of the cavity to the laser frequency at low frequencies, while at high frequencies the length of the cavity is used as a reference to quiet the laser frequency. The crossover between these two paths is near 15 Hz as can be seen in figure 4. The design of the Advanced LIGO triple suspensions allows actuation at each stage with progressively less actuation strength at lower stages. For this reason the different stages of the suspension are used in a hierarchical feedback scheme where lower frequencies are offloaded to higher stages.

3.2 Angular Control

Sensing of the angular degrees of freedom of the input mode cleaner is achieved through the use of differential wavefront sensing[2][8]. The differential wavefront sensing scheme relies on sensing the beat note between the first higher order mode and the fundamental Gaussian mode which is accepted by the cavity. When a tilt or translation exists between the optical

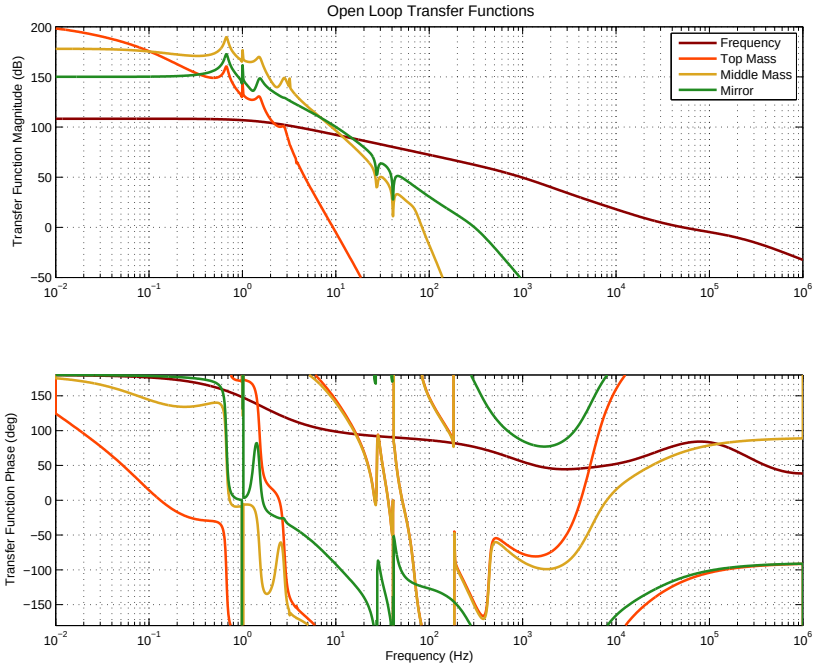

Figure 4: A model of the open loop transfer functions of the various actuators in the input mode cleaner length/frequency control servo. The triple pendulum suspension of the MC2 mirror is used in a hierarchical scheme to control the length of the cavity at low frequency using the laser frequency as a reference. At higher frequencies the length of the input mode cleaner is more stable and the feedback signal is instead used to stabilize the laser frequency.

axis of the input beam and the optical axis of the input mode cleaner the reflected beam from the cavity has a significant fraction of its power in the TEM_{01}/TEM_{10} mode[9].

The TEM_{01}/TEM_{10} mode beats with the sideband light in a unique way due to the fact that the field strength has opposite signs on opposite sides of the beam. This means that the beat note produced with the TEM_{00} mode of the sideband light has opposite signs on opposite sides of the beam. These signs would cause cancellation if the entire beam were collected on a single detector, but a split photodetector is sensitive to this effect. For this reason the Advanced LIGO differential wavefront sensors use a quadrant detector which is sensitive simultaneously to the pitch and yaw modes. In addition to the two differential wavefront sensors a quadrant detector sitting behind MC2 gives absolute information about the input beam relative to the optical bench.

The differential wavefront sensors are placed in the IMC reflected beam with 90° separation in Gouy phase so that the signals are orthogonal. They are not placed with any particular Gouy phase separation from the cavity mirrors, however. Indeed, the total accumulated Gouy phase from the cavity waist is roughly 55° for WFSA and 155° for WFSB.

In a cavity with more than two mirrors, the number of degrees of freedom of the cavity exceeds the two degrees of freedom of an optical beam. The differential wavefront sensors are only sensitive to the *relative* alignment between the optical axis of the input beam and the optical axis of the cavity. This leaves one degree of freedom unsensed in the input mode cleaner. This unsensed degree of freedom can be most concisely stated as the beam spot location on MC3.

The measured sensing matrix is given in table 1 in units of Watts per radian. This measurement agrees reasonably well with simulations in the higher order mode simulation package *Finesse*[7][11].

The high frequency power fluctuations out of the input mode cleaner due to angular fluctuations of the mirrors were found to be low enough that the angular control loops are engaged with very low unity gain frequencies. The control scheme has the mirrors following the input beam by feeding the WFS signals to the cavity mirrors with a 500 mHz unity gain frequency. In addition, a 10 mHz servo adjusts the pointing of the input beam to keep the beam centered on the QPD behind MC2.

	Mirror	WFSA	WFSB
Pitch	MC1	-46	300
	MC2	-863	377
	MC3	-91	291
Yaw	MC1	-413	51
	MC2	72	687
	MC3	453	-80

Table 1: The measured sensing matrix of the angular control loops of the input mode cleaner. Units of the sensing elements are in W/rad. The accumulated Gouy phase from the cavity waist is approximately 55° for WFSA and 155° for WFSB.

3.3 Cavity Pole

If we define the reflectivity of MC1 and MC3 as r and consider MC2 to be completely reflective, then we can express the transmissivity of the IMC as

$$t_{IMC} = e^{ik\ell_3} \frac{-t^2 e^{-ik\phi}}{1 + r^2 e^{-i\phi}}. \tag{3}$$

Here t is the transmissivity of MC1 and MC3, ℓ_3 is the distance from MC1 to MC3, ,$k = \frac{2\pi f}{c}$ is the spatial frequency of the light, and ϕ is given by (2). The cavity is on resonance when $k\ell$ is a equal to $2n\pi + 1$ for any $n \in \mathbb{Z}$. Notice that the transmissivity of the cavity looks identical to that of an impedance matched two mirror cavity except for the static phase shift $e^{ik\ell_3}$.

If we consider the transmissivity of frequencies very near the resonance frequency, then we are justified in Taylor expanding the exponential on the bottom to first order and the one on the top to 0th order. Doing so gives an expression which looks like a single pole transfer function;

$$t_{IMC} \approx e^{ik\ell_3} \frac{\Omega}{\Omega + i\omega}, \tag{4}$$

where

$$\Omega = \frac{1 - r^2}{r^2} \frac{c}{\ell}. \tag{5}$$

This parameter, Ω, is commonly referred to as the cavity pole. Since the losses in a cavity act to reduce the effective reflectivity of the mirrors, a measurement of this parameter is sensitive to the losses in the cavity at the level of the errors in the known mirror reflectivities.

There are many ways to measure the cavity pole; the simplest way for in our experiment was to add a broadband amplitude modulator in between

the laser and the input mode cleaner. To measure the cavity pole we then locked the cavity on the carrier light and added an amplitude modulation sideband which we swept from 500 Hz to 100 kHz. By demodulating a sample of the light before it entered the cavity and comparing it to the demodulated light in transmission of the cavity we were able to measure the cavity pole very precisely (figure 5). It should be noted that measuring the cavity pole in this way requires using two carefully balanced photodiodes otherwise the measurement will be polluted by the relative transfer function of the two photodiodes.

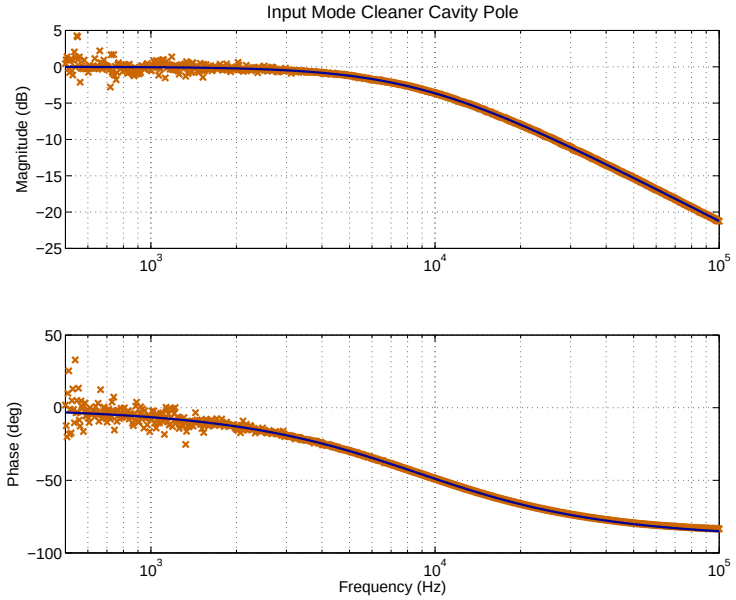

Figure 5: The measured IMC cavity pole is shown together with a fit to (4). The fit has a pole frequency of 8712 Hz which gives a finesse of 522. These values are within the error bars on the measured mirror reflectivities eliminating the possibility of excessive losses.

The results are shown in figure 5 together with a fit to equation (4). The results give a cavity pole of 8712 Hz which is equivalent to a finesse of 522. These numbers are exactly what was expected within the error bars of the measured reflectivity of the mirrors.

3.4 Noise Budget

As with all lock-in experiments, the measured feedback signals to the length and frequency path are a measure of the sensitivity of the input mode cleaner

to length fluctuations. It is important to understand the source of this noise in the cavity measurement because some noise sources are quieted by feedback system while some noises, e.g. sensing noises, are impressed by the control system and show up as noise at the output of the input mode cleaner.

Figure 6 shows the results of our efforts to understand the source of the measured length noise. There are two dominant terms which explain the length noise at low frequencies; seismic noise and damping sensor noise. Seismic noise dominates the low frequency noise but is filtered very steeply above the three suspension resonances. Damping sensor noise is length noise from the shadow sensors used for active damping **Cite Earlier Section** being impressed onto the suspension through the damping loops.

At higher frequencies, above 100 Hz, the measured noise is dominated by vibration of the injection bench of the pre-stabilized laser. The fact that this noise does not perfectly line up with the measured noise is due to the fact that the vibration noise is only measured at one point on the PSL table and the exact coupling is unknown.

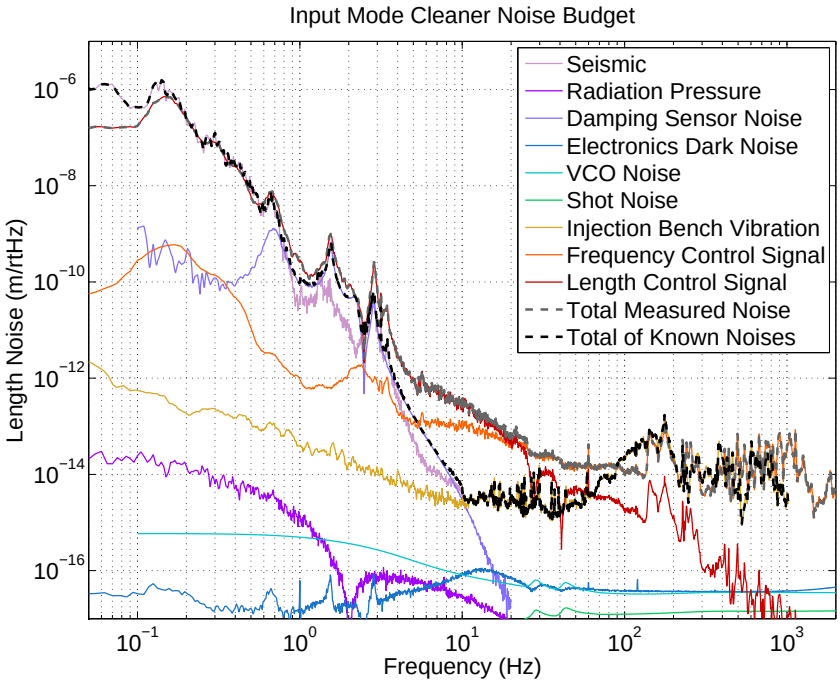

Figure 6: A noise budget for the input mode cleaner showing the measured control signals together with the know noise sources. Known noise sources explain well the measured noise except for the gap between 5 Hz and 80 Hz.

3.5 Absorption Measurements

The absorption in the input mode cleaner can be measured independently of the losses by tracking thermally sensitive properties of the mirrors. In this case we tracked two different thermally sensitive properties; the shift in the local radius of curvature of the optic and the shift in the frequency of the fundamental mechanical eigenmode of the mirror.

The shift in the local radius of curvature of the optic was measured by tracking the higher order mode spacing as a function of power. The spacing of the different higher order modes is dependent on the q parameter of the cavity which is itself dependent on the local radius of curvature of the mirrors. The Winkler et. al.[13] approximation for the local radius of curvature change is

$$\frac{1}{\delta R} = \delta p = \frac{\alpha}{2\pi\omega^2\kappa} P_a, \tag{6}$$

where α is the coefficient of thermal expansion of the mirror, κ is the thermal conductivity, ω is the beam size, and P_a is the power absorbed by the mirror. Assuming that the absorption is uniform across the mirrors and the same for each mirror; ray matrix methods can be used to derive the Gouy phase shift of the cavity as a function of power. This Gouy phase shift can be expressed equivalently as the shift in the frequency location of the 10 peak. With these assumptions and approximations the shift in the location of the 10 peak is given by

$$\delta f_{10} = -135.1 \frac{Hz}{ppm \cdot W}, \tag{7}$$

where the units of ppm is per mirror rather than total.

One of the difficulties with tracking the local radius of curvature change of the optics is that it is only sensitive to the total absorption and does not allow one to distinguish between mirrors. Tracking the fundamental mechanical eigenmode of the mirrors is however sensitive to the absorption of each mirror.

The frequency of each of the three mirror's eigenmodes was first identified by driving the mirror around the frequency expected from FEA simulations. The feedback signal to the laser frequency was used as the readout mechanism. Figure 7 shows the results of tracking the drumhead eigenfrequency of each of the optics during a 120 W power step lasting 75 minutes. The slope of the MC1 and MC2 curves is 2.55 times greater than the slope of the MC3 curve.

Including this relative slope information in the gouy phase shift calculation described above, the frequency shift of the 01 mode for MC3 is $\delta f_{MC3} = 274.6 \frac{Hz}{ppm*W}$ with MC1 and MC2 being a factor of 2.55 times lower. Putting all of this together gives the absorption numbers quoted in table 2.

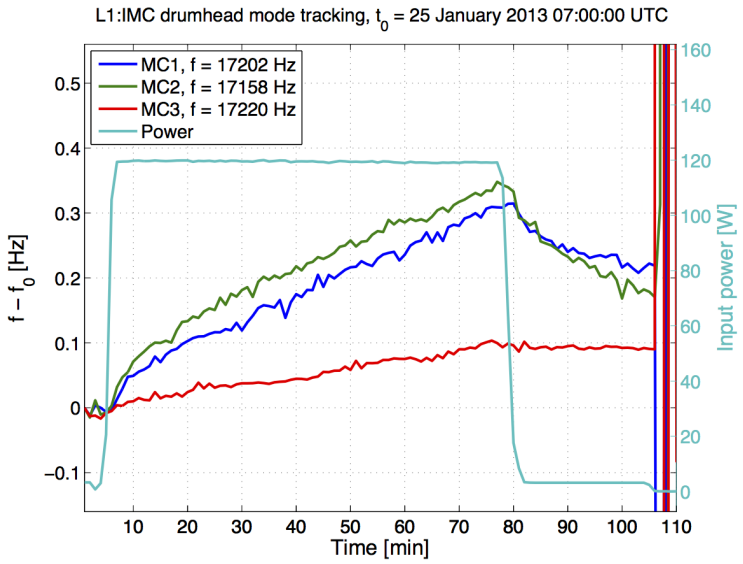

Figure 7: The relative frequency shift of the drumhead eigenmodes of the input mode cleaner optics is shown while the input power was increased to 120 W. The slope of the increase is proportional to the absorption of the optic, but turning the slope into an absolute number is heavily dependent on the material parameters of the optics. Combining the relative slopes with the higher order mode tracking measurement allows for a precise determination of the absorption of each optic.

Optic	Absorption (ppm)	Error (ppm)
MC1	2.11	0.08
MC2	2.11	0.08
MC3	0.83	0.03

Table 2: Measured absorption of the three optics of the input mode cleaner. The relative absorption between the optics was measured with the eigenmode tracking scheme and the total absorption was measured by tracking the higher order mode frequency while changing the power.

3.6 Thermal Lensing

We attempted to track the thermal lensing of the input mode cleaner using digital cameras during high power testing. The digital cameras measured the beam size continuously while the power into the IMC was slowly increased. However; no signal was observed within the accuracy of the beam size measurement on the CCDs.

The Gouy phase tracking absorption measurements allow us to infer the amount of thermal lensing under the same set of assumptions as the absorption measurements. That is to say we assume that the absorption at each mirror is proportional to the slope observed during the eigenmode tracking measurements. We also assume that this absorption shows up as a local radius of curvature change given by the Winkler approximation. Using these adjusted radii of curvature the stable mode in the cavity can be calculated as a function of power. Expanding the result linearly in the input power, the q parameter at the output of the IMC is given by

$$q_{IMC} = -0.2325 + i13.3832 + (6.49 \cdot 10^{-4} - i8.26 \cdot 10^{-4})P, \qquad (8)$$

where P is the input power to the IMC expressed in Watts. If one calculates the overlap between this beam at 0 W input power and this beam at e.g. 100 W of input power, the overlap only drops by 30 ppm indicating that the thermal lensing in the input mode cleaner is negligible.

References

[1] Adhikari, R., Ballmer, S., and Fritschel, P. "Interferometer Sensing and Control Requirements." *Publicly Available Internal Note of the LIGO Collaboration* T070236 (2008).
URL https://dcc.ligo.org/LIGO-T070236

[2] Anderson, D. Z. "Alignment of resonant optical cavities." *Applied Optics* 23 (1984).17: 29442949.
URL http://www.opticsinfobase.org/abstract.cfm?&id=27768

[3] Arain, M., Mueller, G., Martin, R., Quetschke, V., Reitze, D. H., Tanner, D. B., and Williams, L. "Input Optics Subsystem Design Requirements Document." *Publicly Available Internal Note of the LIGO Collaboration* T020020 (2009).
URL https://dcc.ligo.org/LIGO-T020020

[4] Black, Eric D. "An introduction to PoundDreverHall laser frequency stabilization." *American Journal of Physics* 69 (2001).1: 79.
URL http://link.aip.org/link/AJPIAS/v69/i1/p79/s1&Agg=doi

[5] Drever, R. W. P., Hall, John L., Kowalski, F. V., Hough, J., Ford, G. M., Munley, A. J., and Ward, H. "Laser phase and frequency stabilization using an optical resonator." *Applied Physics B* 31 (1983).2: 97105.
URL http://link.springer.com/article/10.1007/BF00702605

[6] Franzen, A. "Uses the vector components library developed by Alexander Franzen; available at http://www.gwoptics.org/ComponentLibrary/." 2010.
URL http://www.gwoptics.org/ComponentLibrary/

[7] Freise, A. "Finesse: Frequency Domain Interferometer Simulation Software." 2013.
URL http://www.gwoptics.org/finesse/

[8] Fritschel, P., Mavalvala, N., Shoemaker, D., Sigg, D., Zucker, M., and Gonzlez, G. "Alignment of an interferometric gravitational wave detector." *Applied Optics* 37 (1998).28: 67346747.
URL http://www.opticsinfobase.org/abstract.cfm?id=61206

[9] Morrison, E., Meers, B. J., Robertson, D. I., and Ward, H. "Automatic alignment of optical interferometers." *Applied optics* 33 (1994).22: 50415049.
URL http://www.opticsinfobase.org/abstract.cfm?&id=42086

[10] Mueller, G. "Pointing Requirements in Advanced LIGO Part I." *Publicly Available Internal Note of the LIGO Collaboration* T020022 (2003).
URL https://dcc.ligo.org/LIGO-T020022

[11] Privitera, S. "Sensitivity Acheived by the LIGO and VIRGO Gravitational Wave During LIGO's Sixth and Virgo's Second and Third Science Runs." *Publicly Available Internal Note of the LIGO Collaboration* T1100338 (2012).
URL https://dcc.ligo.org/LIGO-T1100338

[12] Shoemaker, D. H. "Advanced LIGO Anticipated Sensitivity Curves." *Publicly Available Internal Note of the LIGO Collaboration* T0900288 (2010).
URL https://dcc.ligo.org/LIGO-T0900288

[13] Winkler, W., Danzmann, K., Rdiger, A., and Schilling, R. "Heating by optical absorption and the performance of interferometric gravitational-wave detectors." *Physical Review A* 44 (1991).11: 70227036.
URL http://docuserv.ligo.caltech.edu/docs/public/P/P910012-00.pdf